Plasma Processes in a Low-Pressure Spark Discharge*

H. M. Epstein, W. J. Gallagher, P. J. Mallozzi, and T. F. Stratton†

Battelle Memorial Institute, Columbus Laboratories, Columbus, Ohio 43201
(Received 8 September 1969; revised manuscript received 13 February 1970)

Measurements on a 60-kV 1-μF vacuum spark discharge indicate the following sequence of events. During the early stages of the discharge, the current is carried mostly by electrons which are accelerated to the full tube voltage, as seen from intense bremsstrahlung x-ray production at the anode. The fast electron current and accompanying x-ray emission then diminish, but the total current continues to increase. During the time of reduced x-ray emission, the plasma emits a strong microwave pulse which peaks near the frequencies characterizing the electron drift instabilities. The dense beam of fast electrons then reappears for about 50 nsec and the whole cycle repeats, perhaps twice more. Although the fast electron stream repeatedly appears and disappears, the total current (fast stream plus drift current) usually rises monotonically. When a current of about 4×10^4 A is reached (in $\sim5\times10^{-7}$ sec), dense material vaporized from the anode reaches the cathode and the tube impedance collapses. These events are explained in terms of a model which treats the discharge as alternating between two current modes, one dominated by a fast electron beam, the other by electron drift instabilities.

I. INTRODUCTION

The detailed behavior of an electron current in a high-voltage pulsed linear discharge is unusually difficult to describe. This is due partly to the complex phenomena which combine to produce breakdown and the initial buildup of a space-charge-neutralizing plasma, but mainly to the several varieties of strong interaction between the current and the plasma. These include plasma oscillations, instabilities, particle bunching, plasma turbulence, and heating, all accompanied by a rich spectrum of electromagnetic radiation. At various times coherent microwaves, as well as a nonequilibrium ultraviolet and x-ray spectrum of line radiation, recombination radiation, and bremsstrahlung, are produced. Of particular interest here are the plasma conditions resulting from the combination of a high electric field and low plasma density. With the field sufficiently strong, as in the present experiment, a small group of plasma electrons runs away[1–5] forming a beam which interacts with the bulk plasma. By this interaction the beam momentum is transferred to a drift shared by the plasma electrons. Drift instabilities then produce anomalous resistance and "plasma turbulence." The vacuum or low-pressure spark phenomenology is, thus, closely related to both turbulent heating and beam-plasma studies.

Some of the earlier experiments related to this work were concerned with the development of intense, pulsed x-ray sources.[6–9] In these studies, bremsstrahlung radiation was produced by striking a target anode with large currents of runaway electrons. The phenomenology of this type of discharge was studied by Suladze and Plyutto,[10] who found that the beam current in a pulsed discharge with a plasma cathode developed in two stages. During the first space-charge-limited stage the current increased with the plasma density and was independent of the accelerating field. Subsequent development of the discharge was dominated by an anomalous resistance arising from the current instabilities.

The importance of anomalous resistance in low-pressure discharges links the present work to a broad class of turbulent heating phenomena. The basic concept of this type of turbulent heating is to force a current through a plasma which is so strong that the electron drift energy exceeds the plasma thermal energy and drift instabilities develop.[11] Participation of the plasma ions in the instabilities results in an electrical resistivity very large compared to that for the hot quiescent plasma. Much theoretical and experimental work has been done in this area since the idea of anomalous ohmic heating was first suggested by Zavoiskii[12] and confirmed by Babykin *et al.*[13,14] Anomalous resistance in a strong electric field has been treated theoretically by Buneman[5] and Shapiro,[15] and experimentally by Suprunenko *et al.*[16] and Hamburger.[17] Although no magnetic field other than the self-magnetic-field of the discharge is present in the experiment described here, the instability phenomenology is very similar to those turbulent heating experiments in which the current runs parallel to the magnetic field,[18–23] and to the various pinch discharges. The results of Suprunenko *et al.*[16] are particularly relevant to

the present work in that the main features of the discharge are related to the runaway phenomenon and the drift instabilities. Whenever the applied electric field exceeds the critical electric field for electron runaway, large currents of runaway electrons are produced, together with intense microwave radiation. The runaway electron current and microwaves display a multipeaked behavior, similar to that observed on a faster time scale in the present experiment. These peaks are correlated with the buildup and decay of electrostatic instabilities.

In the present work, emphasis has been put on the investigation of the basic runaway process in a strong electric field, and on the interchange between beam and drift instabilities. No attempt has been made to contain the hot plasma. The heavy atom content of the plasma provides some useful insights on the nonequilibrium ionization and radiation problems as well as the effect of ion mass on discharge resistance.

II. DESIGN OF EXPERIMENT AND DIAGNOSTIC METHODS

The experimental apparatus consists of a 1-μF capacitor with charging voltage variable to 75 kV, a triggered spark gap switch, and a vacuum discharge chamber. The source inductance is 0.12 μH. Details of the discharge geometry are shown in Fig. 1. A molded insulator surrounds the cathode, projecting about 2 mm above the plane metallic cathode surface to provide an electric field which reaches a maximum at the cathode-insulator boundary. The projecting insulator also considerably improves the focus of the electron beam and the uniformity of breakdown. Anode and cathode materials, spacing, and the pressure and composition of the ambient atmosphere in the discharge volume have all been varied in order to assess the importance of these mechanical parameters.

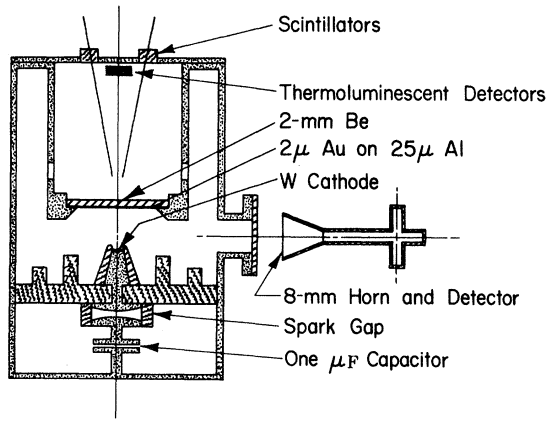

FIG. 1. Discharge chamber (schematic). The spacing between anode and cathode is 1.6 cm unless otherwise indicated. The cathode diameter is 1 cm, and the overall chamber is 20 cm i.d. by 15 cm high.

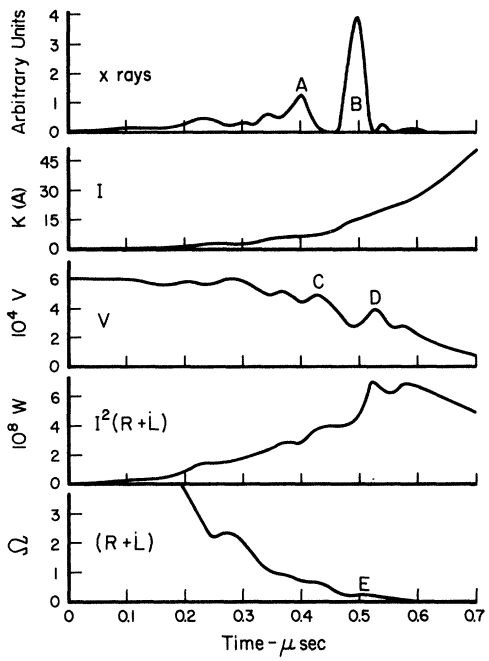

FIG. 2. Composite time histories of anode x rays, current, voltage, power, and resistance.

The electrical properties of the discharge are evaluated from oscillographic records of the voltage, dI/dt, current, and charge. Of principal value are the charge, current, and rate of change of current, which when combined with the charging voltage, the source capacitance, and the source inductance allow an evaluation of the resistive properties of the discharge. The discharge resistance and the instantaneous power delivered to the arc volume, as derived from oscilloscope records, are shown in Fig. 2.

Study of the bremsstrahlung produced at the anode provides a convenient method for evaluating the energy and current of fast electrons reaching the anode. The anode consists of 2 μ of gold plated onto 0.0025 mm of Al, and backed by a Be plate 2 mm thick. Spectrum and intensity of the bremsstrahlung produced as the beam electrons are decelerated in the Au target are directly related to the beam energy and current. The absolute yield of bremsstrahlung x rays is inferred from the energy deposited in a stack of calibrated thermoluminescent detectors (LiF-impregnated Teflon disks). Time-dependent yield and spectral information are derived from the amplitudes of signals received in a matched pair of plastic scintillator-photodiode detectors behind different thicknesses of absorber. The beam voltage as a function of

time may be extracted from the relative amplitudes of the photodiode signals to an estimated accuracy of ± 20%, and this information combined with the absolute integrated yield in the thermoluminescent detectors allows the beam current (for beam energies above 30 kV) to be determined within ± 30%.

Measurements of the x-ray yield from the plasma volume, as differentiated from the anode bremsstrahlung, confirm the presence of low-energy (~1–2-keV) x rays. The yield, which depends strongly on the electrode materials and the tube geometry, is difficult to measure because of the competing signals from the anode bremsstrahlung and from detector bombardment by high-energy electrons capable of penetrating the thin absorber foils necessary for soft-x-ray studies. Plasma temperature is inferred from measurements of these x rays in detectors shielded from the anode radiations. However, since it is impractical to also shield the detectors from the cathode it cannot be assumed that the x rays come only from the plasma volume. It is possible that part or all of the radiation arises from recombinations at the cathode of atoms highly ionized during the resistive portion of the discharge. The soft radiation is observed rather late in the discharge, from $\frac{1}{2}$ to 1 μsec after initiation (Fig. 3). This is the time scale which would be required for ions in the discharge at the time of peak power to reach the cathode. It is also possible that the electron drift velocity is still high enough at late times to create soft bremsstrahlung x rays. This possibility is discussed later.

In the course of inferring the plasma-electron temperature from the emitted x-ray spectrum, it is, in general, necessary to know the details of the emission process. Here, it can only be stated that the dominant x-ray emission is probably

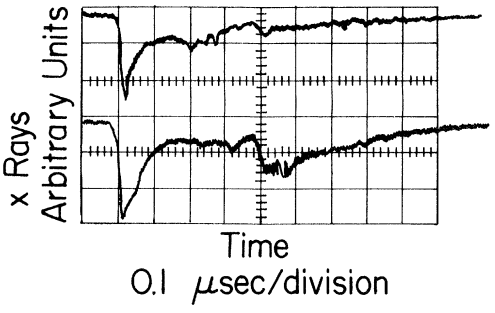

FIG. 3. Plasma x rays behind 0.0025-cm Al (top) and behind 0.005-cm Be (bottom). Dual scintillator-photomultiplier detector system. The time scale is 0.1 μsec/(large division).

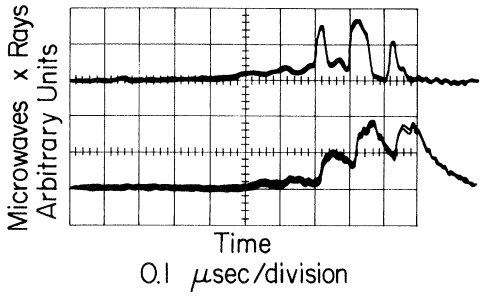

FIG. 4. Composite time history of anode x rays (top) and microwaves with an 8-mm system (bottom).

line radiation, owing to the partly stripped high-Z materials in the plasma. However, since the line spectrum is probably rich over a broad band because of the presence of a mixture of ion species, it is possible to conjecture that the line emission is distributed in a temperature-dependent exponential envelope as suggested by the corona model and then to predict the plasma temperature from the slope of the envelope. Differential foil measurements tend to imply an electron temperature of 0.8 keV using this interpretation.

The emission of microwave radiation from the plasma accompanies the discharge. The oscillographic record of the signal originating in a crystal detector behind a length of 8-mm waveguide oriented with E parallel to the discharge is shown in Fig. 4, where a composite display of anode bremsstrahlung emission and microwave signal is presented. The microwave spectrum in the 1-mm–5-cm range was measured very approximately by cutoff filters and waveguides, and by observing the pulse spread due to frequency dispersion on transmission of the microwaves through 30 m of 3-cm waveguide. Generally, the measured spectrum tends to peak near 10 GHz.

The radial and axial motions of the plasma are derived from streak camera photographs. After an initial fast pinch, the visible discharge remains at a constant radius for about 1 μsec. This radius depends on the plasma composition. Elimination of most of the light cathode insulator materials from the discharge causes the radius to almost double. An example of a radial and an axial streak record is shown in Fig. 5.

The time-dependent spatial distribution of anode x rays is evaluated with a pinhole camera. An array of four matched plastic scintillators with photomultipliers monitored x-ray emission as a function of the discharge radius. The extremely sharp spikes on the oscilloscope traces from the pinhole camera (Fig. 6) are in definite contrast to the rather broad x-ray pulses observed on detectors view-

ing the entire anode. The explanation for this difference might be that the fast electrons causing the x rays are in annular sheets moving radially inward at velocities greater than 10^7 cm/sec. At these high velocities the leading edge of the spikes would appear simultaneously in the detectors, as seen in the experiments.

III. DISCHARGE INITIATION AND GROWTH

A. Cathode Processes

A description of the complete discharge phenomenon requires an understanding of the cathode processes. The plasma physicist may find it convenient to omit this section on a first reading.

The ambient pressure in the discharge tube at the initiation of the vacuum discharge is about 10^{-5} Torr. The conical shape of the projecting cathode insulator provides a field concentration which is sufficient to initiate a discharge at the cathode-insulator boundary. Electrons cascading over the surface of the insulator vaporize a small amount of the insulator material and form a conducting sheath around the insulator at early times. Evidence for the emitting sheath around the cathode may be seen in pinhole photographs exposed by high-energy electrons streaming from the cathode insulator.

In its early phase, the discharge current appears to be limited by the space charge in the cathode region which is only partially neutralized by plasma. Estimates of the importance of the various mechanisms which contribute to electron emission

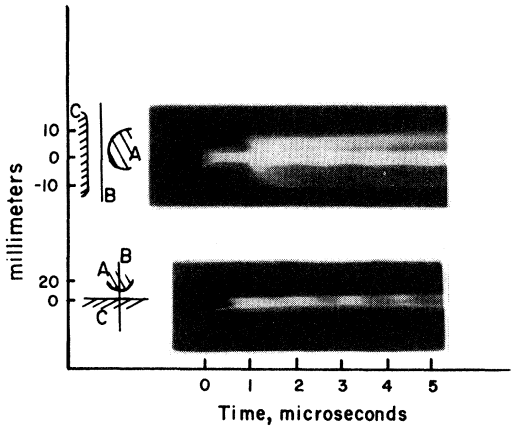

FIG. 5. Streak pictures of discharge at 8.3 mm/μsec. Slit B perpendicular to discharge halfway between anode C and cathode A (top). Slit aligned with the axis of the discharge (bottom).

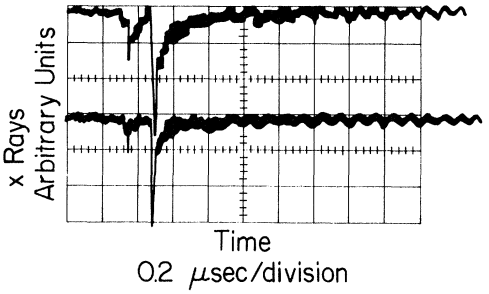

FIG. 6. X rays sweeping past small pinhole camera detectors. Detectors view positions on the anode 1 mm apart.

from the cathode indicate that ion bombardment rather than field or thermionic emission is the most important process at this time. Sternglass[24] relates the yield of secondary electrons per incident ion to the properties of the incident ions and the surface characteristics as follows:

$$\Delta = 35.2 f Z^{2/3}(Z_i/E')^2 \ln(4E'/I) \text{ electrons/ion}, \quad (1)$$

where f is a factor slightly greater than unity which accounts for the contribution to the yield from secondaries formed by the high-energy knock-on electrons (δ rays), and may be approximated by $f = (200 + E')/(100 + E')$. The quantity Z is the atomic number of the target material, I is the mean excitation potential for an atom of the stopping material $E' = (m_e/M_i)E_i$ in electron volts, and E_i and Z_i are the energy and charge of the incident ion. Since the plasma is composed of an undetermined mixture of heavy and light ions from the electrodes and insulator it is only possible to estimate the average ion mass and charge. The value of Δ can range between 10^4 (for incident tungsten ions with an average charge of 10) to 10^3 (for incident carbon ions with an average charge of 4). Space charge limits the ratio of electron to ion current to roughly $(M_i Z_i/m_e)^{1/2}$, which varies from 2×10^3 to 3×10^2 A for these same incident ions. Thus it appears that the rate at which electrons are emitted from the cathode by ion bombardment is greater than the space-charge-limited current, so that cathode emission is not the limiting factor which determines the tube impedance after a plasma is established. Photoemission further increases cathode emission with the buildup of the uv and x-ray flux.

B. Plasma Buildup

The rate of energy deposition at the anode is sufficiently great to cause a dense high-velocity plasma blowoff. Streak camera pictures (Fig. 5)

show a plasma region proceeding from the anode toward the cathode at about 1 cm/μsec, and another plasma region proceeding simultaneously from the cathode toward the anode at about 2 cm/μsec. Lighter atoms from the projecting insulator probably are the main component of the cathode plasma, allowing it to move at a higher velocity than the heavy anode plasma for a given temperature. The plasma between these two advancing fronts is either too tenuous or highly ionized to be seen with the streak camera. The anode and cathode plasmas collide in a time of about 0.7 μsec. The "early-time" regime, as defined here, ends at this time.

Thus, the over-all description at early times appears to include a cathode plasma proceeding across the gap and from the annular insulator inward, a transition plasma in which the electric fields are sufficiently intense to cause a strong "runaway" condition, and a dense anode plasma proceeding across the gap. Most of the discharge electrical resistance should occur in the less dense middle plasma region. Since the current rise time with the system shorted by a copper bar is considerably faster than with the vacuum gap, the discharge impedance, not the storage bank inductance, controls the current during the early time. This impedance, which is dominantly resistive, can come from several effects. (a) cath ode emission limitations, which are probably negligible for the reasons discussed in Sec. III A; (b) space-charge buildup, particularly in the middle or transition region of the discharge; (c) anomalous resistance caused by collective interactions;

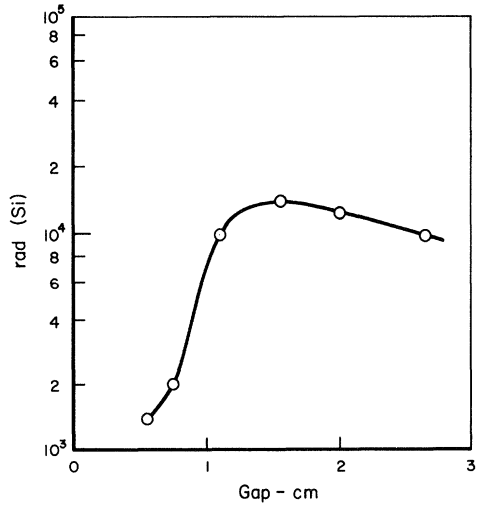

FIG. 7. Integrated yield of anode x rays versus anode-cathode spacing.

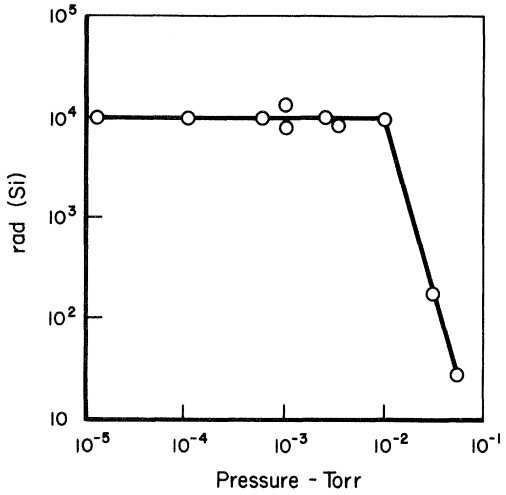

FIG. 8. Integrated yield of anode x ray versus initial nitrogen pressure.

(d) rapidly changing inductance from the collapsing current sheets; and (e) normal plasma resistance within a thin skin depth. Mechanisms (b) and (c) appear to be the significant processes in the discharge phenomena.

In the preceding description, a principal condition is that the discharge is dominantly space-charge limited during the time of interest, the early-time regime. Considering the dense plasma source at the anode and the strong electric field, it is expected that the space-charge limitation would be highly dependent on the distance that the plasma must travel to neutralize the space charge. Assuming the anode plasma to act like a conducting piston, accelerated by an electric field toward the cathode, the time required for traversal of the gap is inversely proportional to the cube of the gap spacing. The rapid decrease in anode bremsstrahlung yield with decreasing separation, shown in Fig. 7, is attributed to this effect.

IV. IMPEDANCE COLLAPSE

The plasma density required to cause impedance collapse can be estimated on the basis of the assumption that the plasma resistance will be drastically reduced when, (i) the instability responsible for the anomalous resistance is eliminated, and (ii) the current is no longer limited by space charge. Since the drift instability diminishes as the plasma temperature approaches the drift energy, this process can avert impedance collapse only for a short time span. Thus, impedance collapse probably occurs when the current is no longer space-charge limited, or when the electron density is greater than that obtained from

$$I = 1.6\times 10^{-19} n_e\, C(2\,kT_i/m_e Z)^{1/2}, \qquad (2)$$

where I is current, T is the ion temperature (assumed to be equal to the electron temperature), n_e is the electron plasma density, and C is between $\frac{1}{2}$ and $\frac{1}{4}$ depending on the ion angular distribution. Substituting (1) into the pinch equation ($I^2 = 200NkT$) gives the number of electrons per cm of the discharge, $N = 1.4$ to $5.6 \times 10^{13} Z$.

The visible discharge radius stabilizes at about 0.1 cm during the time of interest. Thus, assuming an average Z of 10 for the ions and a pinch radius of 0.1 cm, the impedance collapse should occur when the electron density of the plasma arriving from the anode exceeds $\sim 10^{16}$ cm^{-3}. However, when the initial pressure of the ambient gas in the tube is sufficiently high, the above N is exceeded at the initiation of the discharge, a significant discharge resistance will not develop, and the electric field conditions for runaway are not met. This ambient pressure of nitrogen is about 0.01 Torr. Figure 8 shows that the x-ray yield, one indication of the presence of fast electrons, is indeed dropping sharply at 0.01 Torr.

The effect of the ion mass on impedance collapse has also been investigated. As expected, light materials such as Al or Be on the anode result in a faster-moving anode plasma and earlier impedance collapse. An opposite result is obtained when the insulator at the cathode perimeter is coated with lead. In addition to a slower cathode plasma, the restriction of low-Z materials from entering the plasma results in a higher effective Z which permits higher plasma densities before impedance collapse.

V. DISCUSSION

Early-time records of the voltage, current, resistance, dissipated power, and anode x rays for a typical discharge are given in Fig. 2. The current rises monotonically and when a current of about 4×10^4 A is reached ($\sim 5 \times 10^{-7}$ sec) the impedance of the discharge collapses to a very low value. Until the impedance collapse the discharge is mainly resistive ($IR > LI^{\cdot}$), but the nature of the current undergoes several abrupt changes, as is evidenced by the x-ray peaks seen at points (A) and (B). Analysis of the intensity and spectrum of the thick-target x-ray bremsstrahlung from the anode indicates that most of the current at those times is carried by a small subgroup of fast electrons which are accelerated to approximately the full tube voltage. The tube voltage passes through relative minima at nearly the exact x-ray peaks, indicating that the plasma tends to present less resistance to current when the current is in the "beam" mode. This tendency is clearly evidenced by inflections and relative minima at the corresponding points on the resistance curve; but the main feature of the resistance curve is the persistent decrease with time, because of the gradual buildup of plasma density and the resulting increase in space-charge neutralization of the current. Another important feature shown in Fig. 2 is the sharp decrease in x-ray output after each x-ray maximum followed by a rise of voltage to a relative maximum, as seen at points (C) and (D).

These and several other features of the over-all plasma response are readily interpreted with the assumption of a collective interaction between the fast electron beam and the electrons of the bulk plasma. The average beam density n_b at the fast current peaks (A) and (B) is calculated from the measured currents, voltages, and areas of the discharge, to be $\sim 10^{14}$ and $\sim 3 \times 10^{14}$ cm^{-3}, respectively. On the other hand, the pinch balance equation indicates that for kilovolt temperatures the bulk plasma electron density n_e at those two points is $\sim 4 \times 10^{15}$ and $\sim 3 \times 10^{16}$ cm^{-3}. In the "cold beam" approximation the electric field vectors of the longitudinal Langmuir waves excited by the beam increase in amplitude in proportion to $e^{\gamma t}$, with the growth rate[25]

$$\gamma \sim (n_b/n_e)^{1/3}\, \omega_{pe} \text{ sec}^{-1}, \tag{3}$$

where ω_{pe} is the electron Langmuir frequency. The beam-plasma interaction is thus capable at both points of disrupting the beam in a time of order 10^{-12} sec. The fact that the duration of the fast current pulses is generally 20–50 nsec is probably due to the velocity spread of the beam.[15] The nature of the fast current pulses may thus be explained as follows.

The electron beam interacts with the electrons of the bulk plasma via a collective beam-plasma interaction and excites longitudinal electron plasma oscillations of frequency $\sim \omega_{pe}$. The Langmuir oscillations then "scatter" the beam, disrupt it in approximately 20–50 nsec, and die out themselves almost immediately after the beam disappears. A possible explanation for the rapid disappearance of the Langmuir waves is nonradiative decay due to the effect of over-all macroscopic plasma inhomogeneity. The decay time due to this mechanism of Langmuir waves in an inhomogeneous plasma is[26]

$$\tau_L^{-1} \sim \lambda_D \mid \text{grad } \omega_{pe} \mid , \tag{4}$$

where λ_D is the Debye radius. Since the plasma radius $R \sim 0.1$ cm is fairly constant during most of the discharge and the electron thermal velocity $v_e = \sqrt{(kT_e/m)}$ is typically $\sim 10^9$ cm/sec,

$$\tau_L \sim R/\lambda_D \omega_{pe} \sim R/v_e \sim 10^{-10} \text{ sec}, \tag{5}$$

which is sufficiently short to justify the neglect of

Langmuir oscillations at times other than during the fast current pulses. Other decay mechanisms may conceivably be stronger than the one considered, but Eq. (5) nevertheless verifies that the Langmuir waves quickly die out.

Strong support for the view that the fast current pulses are stopped by the beam-plasma interaction rather than one of the electron "drift" instabilities is provided by the following considerations. The beam-plasma interaction is essentially an interaction between electrons, which means it has no direct effect on the electron current and tube resistance. The drift instabilities, on the other hand, arise from interactions between electrons and ions and thus do affect the electron current and tube resistance. In this respect, the situation is analogous to that which prevails in quiescent plasmas, where the current and ohmic resistance are influenced by electron-ion collisions, but not electron-electron collisions. Keeping this in mind, the fact that the tube voltage remains relatively low throughout the rise and decay of the fast current pulses in Fig. 2 indicates that the mechanism which stops the beam is "nonresistive," supporting the view that the stopping mechanism is the beam-plasma interaction rather than an electron drift instability. Further indication that the beam-plasma interaction is the main stopping mechanism is the fact that the total current is nearly always increasing with time, even during the extinction of the fast current pulse; this is what one would expect for beam-plasma interactions, which fundamentally derive from the current conserving electron-electron forces. Still further indication is found in the microwaves emitted by the plasma. A characteristic feature is that the measured microwave power peaks shortly after each fast current pulse (Fig. 4), and is relatively low during the pulse. These microwaves tend to spectrally peak near the characteristic electron drift frequencies $(Zm/M)^{1/2}\omega_{pe}$ or $(Zm/M)^{1/3}\omega_{pe}$. (The microwave spectrum is not known with sufficient precision to differentiate between the characteristic frequencies.) This suggests that the current is limited between fast current pulses by one of the drift instabilities, but also tends to rule out these instabilities as a stopping mechanism for the fast current pulses. The sequence of events that follows the fast current peak at point (A) in Fig. 2 may thus be explained as follows.

The electron beam interacts with the electrons of the bulk plasma via a collective beam-plasma interaction and generates growing Langmuir oscillations which scatter and stop the beam without increasing the tube resistance, and then quickly die out. Since the beam-plasma interaction conserves electron current, the beam electrons suddenly impart their momentum to the electrons in the bulk plasma. This increase in electron drift is followed by a voltage rise and a large increase of microwave radiation at the characteristic frequency range of the electron drift instabilities. Between fast current peaks the current is limited by electron drift instabilities which are responsible for the over-all high anomalous resistivity of the plasma and heat the plasma by converting the ordered drift energy into random thermal motion. The relatively high voltage between the fast current peaks may be attributed to the action of the anomalous resistance on the large drift current. The appearance of new fast current pulses is attributed to the intense ohmic heating arising from the anomalous resistance. As the electron temperature is raised a small subgroup of electrons in the Maxwellian tail may again "run away" from the "turbulence forces" associated with the anomalous resistance and form a new beam of fast electrons. In this sense, the phenomenon may be analogous to ordinary electron runaway, where the electrons in the Maxwellian tail are pulled away from the Coulomb scattering associated with the ordinary plasma resistance. After the new fast current appears the whole series of events is repeated, although at higher plasma densities.

We now turn to the plasma state between fast current pulses. Here the most likely mechanism for current limitation is strong plasma turbulence arising from the hydrodynamic[27] (or high-frequency) drift instability. The growth of this instability in the presence of a strong electric field was studied in some detail by Buneman[5] and Shapiro.[15] The calculations have been extended by Mallozzi, Epstein, and Gallagher,[28] who derived the following formula for the effective collision time τ_c of the drifting electrons:

$$e^{\alpha\tau_c} = \beta(E/E_q)^3\tau_c^{7/2} \quad . \tag{6}$$

Here $\tau_c = \omega_{pe}t_c$, $E_q = n_e^{2/3}e$, and α and β are functions of the parameter Zm/M. The dc conductivity associated with such a collision time is

$$\sigma_{(\mathrm{esu})} = (\omega_{pe}^2/8\pi)t_c = (\omega_{pe}/8\pi)\tau_c \quad . \tag{7}$$

The physical mechanism underlying this anomalous conductivity is that the current is disrupted by waves which grow at the rate $\sim(Zm/M)^{1/3}\omega_{pe}$, with wave numbers $k \sim \omega_{pe}/u$ and frequencies $\omega \sim (Zm/M)^{1/3}\omega_{pe}$. For a broad range of conditions we may picture the strong field creating a drift for approximately $10(M/Zm)^{1/3}$ Langmuir plasma periods, after which time the instability randomizes the drift energy into thermal energy. The drift then builds up again and the whole process is repeated, though at a higher temperature. A necessary condition for this state of anomalous resis-

tance or "turbulent heating" to prevail is that the drift velocity be greater than the electron thermal velocity $\sqrt{(kT_e/m_e)}$. The plasma conditions near the typical resistance peak at point (E) of Fig. 2 may be interpreted on the basis of Eqs. (6) and (7) for the anomalous conductivity together with the plasma density $n_e \sim 10^{16}$ cm^{-3} and the assumption (to be discussed later) that the effective charge Z of the ions is ~10. The reasons are the following. The pinch balance equation predicts that $n_e \sim 10^{16}$ cm^{-3} when it is assumed that the plasma reaches kilovolt temperatures and that only $\sim \frac{1}{2}$ of the total current actually flows through the pinch. Now if 10^{16} cm^{-3} is used in Eqs. (6) and (7) for n_e, the measured value of plasma resistance agrees with the theoretical value only if the current is assumed to flow through an area which is approximately $\frac{1}{100}$ of the over-all plasma area. A small runaway region at the center of the discharge has been observed in other experiments.[16,18] The self-consistency of the anomalous resistance description becomes evident when the electron density and calculated current area are inserted into the current equation, leading to an average drift velocity somewhat below 10^{10} cm/sec or electron drift energies < 30 keV. Such a drift is faster than the electron thermal velocity associated with kilovolt plasma temperatures (which justifies the anomalous resistance assumption), yet slow enough to explain the relatively low x-ray output. Further corroboration for the validity of the anomalous resistance picture is that intense microwave radiation is detected at the frequencies characteristic of the high-frequency drift instability at the plasma density $n_e \sim 10^{16}$ cm^{-3}.

As justification for ignoring the low-frequency drift instability, in which the electron drift is disrupted by growing ion oscillations, we note that this instability grows only if $T_i \ll T_e$. Since there are many times more electrons than ions and the instability tends to heat the ions, it is clear that the instability cannot be responsible for more than a small fraction of the plasma heating without destroying the conditions necessary for its growth.

The effective charge of the ions remains uncertain. This is due in part to the uncertainty in free-electron temperature $T_e(t)$, but is mainly due to the ions having insufficient time to strip down to the quasisteady ionization state commensurate with $T_e(t)$, so that $Z(t)$ is not predictable by an equilibrium or steady-state model. In the reported temperature and density regime, the time τ_i required for $Z(t)$ to relax to its quasisteady value is given for the formula[29]

$$\tau_i \sim 10^{12}/n_e \quad . \tag{8}$$

This simple formula is independent of T_e and holds with order-of-magnitude accuracy for any n_e and T_e within its domain of validity. Substitution of $n_e \sim 10^{16}$ cm^{-3} in Eq. (8) leads to an equilibration time of 10^{-4} sec, which is at least a factor of 100 longer than the duration of the discharge. The resulting uncertainty in effective Z is somewhat mitigated by the fact that it enters into the α of Eq. (6) only via $Z^{1/3}$.

VI. CONCLUSIONS

The present experimental evidence suggests that the vacuum or low-pressure spark discharge can be described with a model in which the current alternates between two distinct modes. The beam mode originates with the acceleration of a small group of electrons by the strong electric field; the beam then interacts with the bulk plasma and is stopped by the beam-plasma instability. The drift mode starts when the beam momentum is transferred to the electrons of the bulk plasma. The drift current is limited by anomalous resistance until the plasma heating allows a new subgroup of fast electrons to break away from the turbulence forces associated with anomalous resistance.

ACKNOWLEDGMENTS

The authors wish to thank C. T. Walters and R. D. Wood for their assistance with the experiments.

---

*Work supported in part by the Defense Atomic Support Agency.

†Present address: Los Alamos Scientific Laboratory, Los Alamos, N.M.

[1]H. Dreicer, Phys. Rev. 115, 238 (1959).

[2]H. Dreicer, Phys. Rev. 117, 329 (1960).

[3]L. Spitzer, Nature 181, 221 (1958).

[4]A. Gibson, in *Proceedings of the Third International Conference on Ionization Phenomena in Gases, Venice*, 1957, p. 365 (unpublished).

[5]O. Buneman, Phys. Rev. 115, 503 (1959).

[6]Ch. M. Slack and L. F. Ehrke, J. Appl. Phys. 12, 115 (1941).

[7]W. Schaafs and K. A. Herrmann, Z. Angew. Phys. 6, 23 (1954).

[8]S. K. Handel and J. M. Berg, Arkiv Fysik 21, 1 (1966).

[9]S. K. Handel, Arkiv Fysik 28, 27 (1965).

[10]K. V. Saladze and A. A. Plyutto, Sov. Phys. Tech. Phys. 12, 48 (1967).

[11]T. E. Stringer, J. Nucl. Energy 6, 267 (1964).

[12]E. K. Zavoiskii, Atomic Energy 14, 57 (1963).

[13]M. A. Babykin, P. P. Gavrin, E. K. Zavoiskii, L. I. Radakov, and V. A. Skoryupin, Zh. Eksperim. i Teor.

Fiz. 42, 936 (1962) [Soviet Phys. JETP 20, 1073 (1965)].
[14]M. A. Babykin, P. P. Gavrin, E. K. Zavoiskii, C. L. Nedoceev, L. I. Rudakov, and V. A. Skoryupin, *Plasma Physics and Contributions to Nuclear Research* (IAEA, Vienna, 1966), Vol. I, p. 851.
[15]V. D. Shaprio, Zh. Eksperim. i Teor. Fiz. 44, 613 (1963) [Soviet Phys. JETP 17, 416 (1963)].
[16]V. A. Suprunenko, E. A. Sukhomlin, and N. I. Reva, J. Nucl. Energy 7, 297 (1965).
[17]S. M. Hamburger and M. Friedman, Phys. Rev. Letters 21, 10 (1968).
[18]T. H. Jensen and F. R. Scott, Phys. Fluids 11, 1809 (1968).
[19]P. I. Blinov, L. P. Zakatov, A. G. Plakhov, R. V. Chikin, and V. V. Shapkin, Zh. Eksperim. i Teor. Fiz. 52, 670 (1967) [Soviet Phys. JETP 25, 3439 (1967)].
[20]S. M. Krivoruchko and Yu. V. Medvedev Zh. Tekhn. Fiz. 38, 87 (1968) [Sov. Phys. Tech. Phys. 13, 61 (1968)].
[21]A. P. Babichev, A. I. Karchevskii, Yu. A. Muromkin, and E. M. Buryak, Zh. Eksperim. i Teor. Fiz. 53, 1 (1967) [Soviet Phys. JETP 26, 1 (1968)].
[22]M. V. Babykin, P. P. Gavrin, E. K. Zavoiskii, S. L. Nedoceev, L. I. Radakov, and V. A. Skoryupin, Zh. Eksperim. i Teor. Fiz. 52, 643 (1967) [Soviet Phys. JETP 25, 421 (1967)].
[23]Y. Matsukawa, Y. Nakagawa, and K. Watanabe, J. Phys. Soc. Japan 4, 196 (1968).
[24]E. J. Sternglass, Phys. Rev. 108, 1 (1957).
[25]Ya. B. Fainberg, J. Nucl. Energy 4, 203 (1962).
[26]B. B. Kadomtsev, *Plasma Turbulence* (Academic, New York, 1965).
[27]The term "hydrodynamic instability" as used here refers to the instability derived from standard hydrodynamic equations. In contrast, the low-frequency drift instability treated by G. Field and B. Fried [Phys. Fluids 7, 1937 (1964)] is a microinstability, since its theoretical origin lies in the solution of the detailed microscopic plasma equations (specifically, the collisionless Boltzmann equations) governing the particle distribution functions.
[28]P. J. Mallozzi, H. M. Epstein, W. J. Gallagher (unpublished).
[29]R. W. P. McWhirter, in *Plasma Diagnostic Techniques*, edited by R. H. Huddlestone and S. L. Leonard (Academic, New York, 1965), Chap. 5.

PHYSICAL REVIEW A VOLUME 2, NUMBER 1 JULY 1970

One-Dimensional System of Bosons with Repulsive δ-Function Interactions at a Finite Temperature T

C. P. Yang*
The Ohio State University, Columbus, Ohio
(Received 22 August 1969; revised manuscript received 6 February 1970)

The equilibrium thermodynamics of a one-dimensional system of bosons with repulsive δ-function interaction is found to be intermediate between those of a one-dimensional free-boson and a one-dimensional free-fermion system. Numerical comparisons are given.

I. INTRODUCTION

In a previous paper (which we shall henceforth call I)[1] a method was developed in which the pressure P at any temperature T of a system of bosons with repulsive δ-function interaction in one dimension was shown to be exactly given by

$$P = T/2\pi \int_{-\infty}^{\infty} dk \ln(1 + e^{-\epsilon(k)/T}) , \tag{1}$$

where $\epsilon(k)$ is the unique solution of the integral equation

$$\epsilon(k) = -A + k^2 - \frac{Tc}{\pi}\int_{-\infty}^{\infty} \frac{dq}{c^2 + (k-q)^2} \times \ln\{1 + \exp[-\epsilon(q)/T]\} , \tag{2}$$

with c = interaction strength > 0 and A = chemical potential. We shall in this paper discuss the thermodynamics of such a gas.

II. THERMODYNAMICS

A. Behavior of the Pressure

In terms of the fugacity $z = e^{A/T}$ the pressure of a one-dimensional system has the general form

$$\frac{PL}{T} = \ln\left(\sum_{N=0}^{\infty} z^N \sum_{\text{state } s} e^{-E_s/T} \right) ,$$

where L = size of the one-dimensional system and E_s is the energy of state s. In the present case, it is obvious that E_s increases with increasing c. The coefficient of z^N thus decreases with increasing c. For constant z we therefore have $P(c=0) > P(c \text{ finite}) > P(c=\infty)$, from which follows:

Theorem 1

$$P_{BE} > P(c) > P_{FD} \text{ at a particular } T \text{ and } z. \tag{3}$$

Here P_{BE} and P_{FD} stand for the pressure at a fixed

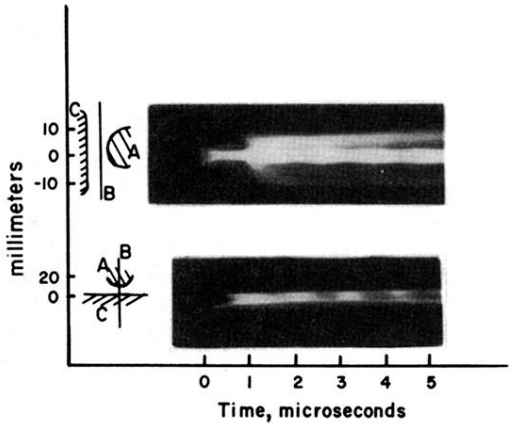

FIG. 5. Streak pictures of discharge at 8.3 mm/μsec. Slit B perpendicular to discharge halfway between anode C and cathode A (top). Slit aligned with the axis of the discharge (bottom).